Thermal Stress Development in a Nickel Based Superalloy During Weldability Test

A computational model was used to quantify the thermomechanical conditions associated with weld solidification cracking

BY Z. FENG, T. ZACHARIA, AND S. A. DAVID

ABSTRACT. A finite element model has been developed to quantitatively evaluate the local thermomechanical conditions for weld metal solidification cracking in a laboratory weldability test (the Sigmajig test). The loading mechanism in the Sigmajig test was simulated by means of nonlinear spring elements. The effects of weld pool solidification on the thermal and mechanical behaviors of the specimen were considered. An efficient algorithm was developed to include the solidification effects in the material constitutive relations. Stress/ temperature/location diagrams were constructed to reveal the local stress development behind the traveling weld pool where solidification cracking occurs. Based on the concept of the material resistance to cracking and the mechanical driving force for cracking, the calculated local stress in the solidification temperature range was used to explain the experimentally observed cracking initiation behaviors of a nickel-based superalloy single crystal under different welding and loading conditions.

Introduction

Weld solidification cracking (hot cracking) is one of the major forms of weld defects that develops during the weld fabrication process. It has been well recognized that solidification cracking during welding, ingot casting, and continuous casting have the same root — from the combined effects of metallurgical and mechanical factors. Metallurgical factors relate to the conditions of solidification, grain size, presence of low melting constituents, etc. Mechanical factors relate to the conditions of stresses/strains developed in weld metal during solidification, as a result of solidification shrinkage and nonuniform temperature changes at positions in and around the weld (Ref. 1).

Research efforts over the past forty years have revealed a comprehensive but qualitative picture about the nature of weld metal solidification cracking. For common engineering alloys, weld pool solidification is a nonequilibrium process which results in the formation of a dendritic microstructure under conditions of constitutional supercooling. During the later stage of the solidification process, there exists a brittle temperature range (BTR) in which the strength and ductility of the alloy are very low, as low melting point constituents segregate between dendrites and form liquid films. At the same time, tensile stresses/strains arise from solidification shrinkage, thermal contraction of parent metal and external restraints. Like many other cracking problems, solidification cracking occurs when the mechanical driving force exceeds the material resistance to cracking (primarily influenced by alloy composition, welding process, and heat input). The mechanical driving force is influenced by welding process, heat input, joint configuration and rigidity, and the thermomechanical properties of alloys.

KEY WORDS

Solidification Cracking Modeling
Weldability Modeling
Finite Element Method
Sigmajig Test
Superalloy
Thermal Stresses
Heat Transfer

In order to understand the solidification cracking problem, both the solidification behavior and the thermomechanical behavior during welding must be evaluated. In the past, studies have been conducted from these two different perspectives. Most studies, however, have focused on the metallurgical factors, that is, the low strength and ductility of the alloy during solidification. Until recently (Refs. 2–4), progress in understanding of the mechanical effects, namely, the thermal stress/strain conditions associated with solidification cracking (the mechanical factors), has been very limited and experimental in nature (Refs. 5–8). The cracking driving forces for different situations could not be compared systematically. In addition, some parameters — such as local cooling rate in the weld pool and its influence on the solidification behavior (thus the material resistance to cracking) — are not available for different situations, due to the lack of heat transfer analysis in the vicinity of the weld pool.

Laboratory weldability tests have been used to study the weld metal solidification cracking phenomena (Ref. 9). During the past half century, many different weldability tests have been devised with completely new or modified tests under continuous development. Despite this, laboratory weldability test results often do not reflect field experience. It can be argued that one of the primary difficulties in applying the weldability testing results to actual welding fabrications is the lack of quantitative assessment of the local stresses/strains within the solidification region during welding.

The Sigmajig test (Ref. 10) is a hot crack test commonly used for sheet metal. The test uses a preapplied load

Z. FENG is with the Edison Welding Institute, Columbus, Ohio; T. ZACHARIA and S. A. DAVID are with the Oak Ridge National Laboratory, Oak Ridge, Tenn.

during welding and determines a threshold stress above which a centerline crack initiates. The threshold stress has been shown to he sensitive to variations in the alloy's composition, welding processes and parameters, and is used as a quantitative index for an alloy's susceptibility to cracking. The consensus is that 1) the higher the threshold stress, the more resistant to cracking the alloy will be; and 2) cracking should not be expected in the Sigmajig test when the preapplied stress level is below the alloy's threshold. However, it needs to he recognized that the prestress is not the local stress acting at the trailing edge of a traveling weld pool where solidification cracking occurs. In the past, few attempts have been made to correlate the external preapplied stress to the local stress/strain field at the crack initiation site.

In the development of a nickel-based superalloy, the weldability of the alloy was characterized using the Sigmajig test. When the test was conducted without applying a load, some alloy compositions exhibited a severe tendency for weld centerline solidification cracking. However, with preapplied load, the threshold stress values could be measured as high as 200 MPa. Similar results were also reported for FeAl alloys (Ref. 11). These experimentally observed phenomena are difficult to interpret without considering the local stress/strain conditions in the BTR.

As a continuing effort to quantify the thermomechanical contributions to solidification cracking, this study provides a detailed finite element analysis of the dynamic development of the local thermal stresses at the trailing edge of the moving weld pool that influence the formation of solidification cracking in the Sigmajig test. The experimentally observed crack initiation behavior under various welding and loading conditions is explained according to the local stress evolutions obtained from the computational models.

Experimental Techniques

Material

The material used in this study was an experimental nickel-based superalloy single crystal. The nominal composition was 15Cr-8.5Co-1.75Mo-2.5W-1Ta-3.5Al- 4.5Ti-0.9Nh (wt-%), similar to that of IN-738 (Ref. 12). The 0.79-mm-thick, 50 by 50 mm^2 Sigmajig test specimens were cut from a single crystal casting in the plane normal to the [001] crystal growth direction. The edges of the specimen were along [100] and [010] directions. The dendritic microstructure of the casting was preserved in the specimen prior to welding. The solidification temperature range of the alloy was determined using the differential thermal analysis (DTA). The on-cooling bulk liquidus and solidus temperatures of the alloy were 1601 and 1404 K, respectively, measured at a cooling rate of 0.33 K/s.

Welding and Sigmajig Testing

An autogenous gas tungsten arc (GTA) weld was made along the centerline of a specimen, *i.e.*, along the [100] crystallographic direction of the single crystal. The welding was performed using a Hobart Cyber-Tig II welding power source and a 1.6-mm (0.0625-in.), 2% thoriated tungsten electrode. Two welding speeds, 10 in./min (4.23 mm/s) and 35 in./min (14.8 mm/s), were selected to study the effect of welding speed on the occurrence of cracking. The welding current was set at 32 A for the low welding speed (4.23 mm/s) and 75 A for the high welding speed (14.8 mm/s). The arc length was set at 0.031 in. (0.79 mm). The arc voltage was dependent on the actual arc length and welding speed, which varied from 10 to 10.5 V in the high-speed tests and 8.5 to 9.5 V in the low-speed tests. Argon shielding gas was used during the test to protect the weld pool. The copper chill block usually placed beneath the specimen to control the weld width was removed during the test in order to avoid analyzing the complex contact heat loss from the block. With the above welding parameters, full joint penetration welds were obtained in all tests.

The Sigmajig test fixture is shown schematically in Fig. 1. The prestress was maintained by the two Bellville washer stacks in the load train. This loading arrangement gives a displacement/load curve with a slope of 6.167 x 10^{-4} mm/N (0.108 mils/lb_f) for each stack of the washers (Ref. 10). In order to apply a tensile stress to the specimen, the stacks of washers were tightened against the steel grip prior to welding, *i.e.*, subjecting a compressive load and shortening its length. In this sense, the loading train of the Sigmajig test can be considered as precompressed "push" springs in the computational models. Because of the thermal expansion/contraction of the specimen, the actual stress applied to the specimen by the loading train is expected to fluctuate around the prestress level during the test.

Two prestress levels were selected: 10 ksi (68.9 MPa) and 25 ksi (172 MPa). In addition, some specimens were welded under the stress-free condition: the specimens were simply laid on the bottom steel grips without the top steel grips being tightened up against the bottom ones. Thus, the restraining effect from the loading fixture did not exist in the stress-free tests. A total of six combinations of loading (restraint) and welding conditions were investigated.

In some tests, the initiation and propagation of the crack were visually monitored using a stroboscopic vision system.

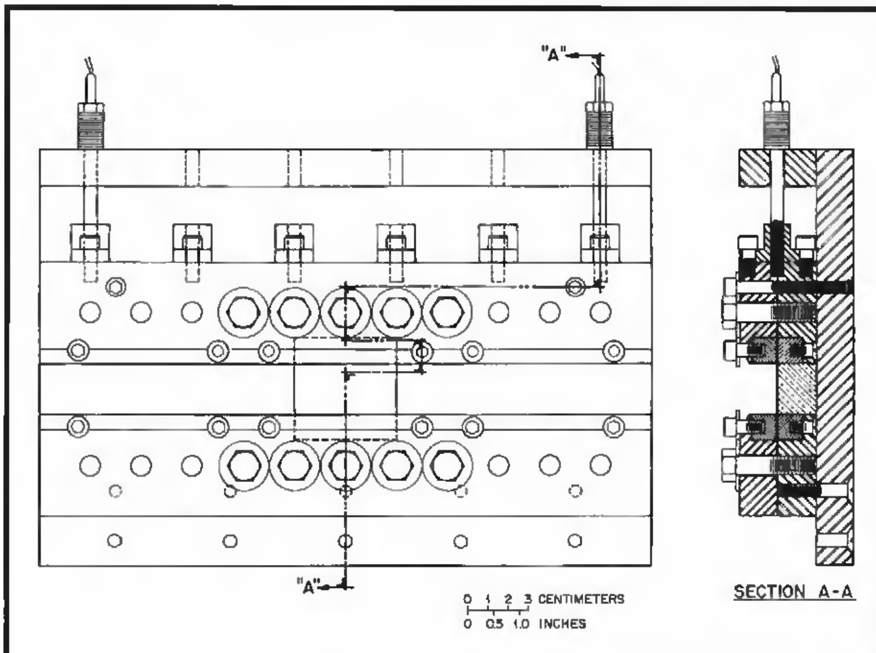

Fig. 1— Schematic representation of the Sigmajig test fixture (Ref. 10).

The details of the vision system have been described in Ref. 3.

Computational Model

For the system under consideration, it is not necessary to solve for the temperature and stress fields simultaneously since the dimensional changes are negligible and the mechanical work done is insignificant compared to the thermal energy from the welding arc (Refs. 13, 14). In this study, the heat transfer analysis was first conducted independent of the stress analysis. The temperature history obtained from the heat transfer analysis was then used as the thermal loading in the stress simulation. It was further assumed that the specimen does not crack in the mechanical model. Finite element formulation formed the basis for this analysis.

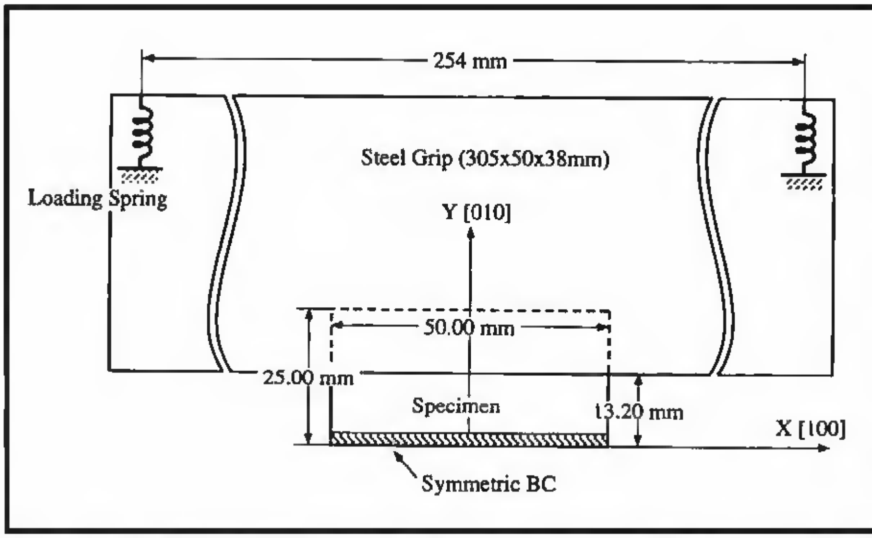

Fig. 2 — Geometric representation of the Sigmajig test and boundary conditions in computational models.

Heat Transfer Model

Since full penetration welds were obtained in the test, the heat transfer in the specimen was modeled as a two-dimensional heat conduction problem. A symmetric half of the single-crystal plate was discretized with four-node linear isoparametric quadrilateral elements, which are more suitable for the problems involving latent heat effect (Ref. 15). Smaller elements were used near the fusion zone. The heat flux from the moving welding arc was assumed to have a spatial distribution of radial symmetric Gaussian profile in the plane of the plate, but uniformly distributed over the entire thickness of the plate, which can be expressed as:

$$q_{arc}(x,y,t) = \frac{3\eta VI}{\pi H r_b^2}\exp\left\{\frac{3\left[(x-x_0-vt)^2+y^2\right]}{r_b^2}\right\} \quad (1)$$

where H is the thickness of plate, V is the welding voltage, I is the welding current, and v is the welding speed. A constant arc efficiency, η, of 70% was used for gas tungsten arc welding (GTAW). The arc beam radius, r_b, was taken to be the same as the electrode diameter (1.6 mm).

In the above equation, it was assumed that the x-axis was along the centerline of the weld bead, and the origin of the coordinate system was located at the center of the specimen—Fig. 2. The welding arc was started at $x = x_0$ (x_0<–25 mm), a location on the run-on copper tab, and moved in the positive direction along the x-axis. In addition, the effect of the steel grips on the temperature distribution of the specimen was assumed to be negligible and thus was not taken into account in the heat transfer analysis.

The convective and radiative heat losses from the surfaces of the plate were considered, whereas the heat loss from the edges of the plate was ignored. Thus, all of the boundary conditions, *i.e.*, the heat loss from the plate surfaces and the heat flux from the arc, can be incorporated into the heat diffusion equation in terms of internal heat generation or loss (body heat flux), Q:

$$\frac{\partial}{\partial x}\left(\kappa\frac{\partial T}{\partial x}\right)+\frac{\partial}{\partial y}\left(\kappa\frac{\partial T}{\partial y}\right)+Q=\rho C_p\frac{\partial T}{\partial t} \quad (2)$$

and

$$Q = -\frac{2h(T-T_\infty)+2\sigma\varepsilon\left(T^4-T_\infty^4\right)}{H}+q_{arc}+q_i \quad (3)$$

where T is the temperature, κ is the thermal conductivity, ρ is the density, C_p is the specific heat, h is the convective heat transfer coefficient, σ is the Stefan-Boltzmann constant, and ε is the radiation emmissivity. T_∞ is the ambient temperature, which was assumed to be 300 K, and q_i is an internal heat generation term.

Due to the experimental nature of the single crystal used in the study, the thermophysical properties were not readily available. The values adopted in the computational analyses were the average values based on the data for several superalloys with similar compositions (Refs. 16–19). Temperature dependent thermal conductivity and specific heat were used, as shown in Fig. 3. In order to account for the increased convective heat transfer by the molten metal flow in the weld pool, the thermal conductivity was enhanced linearly from the solidus (1404 K) to the liquidus (1601 K) and remained constant above the liquidus. The conductivity value for the liquid was five times that at the solidus temperature. A constant density of 8.11 g/cm^3 was taken for the entire temperature range. The convective heat transfer coefficient, h, and the radiative emissivity, ε, were assumed to be 84 W/m^{2}K and 0.2, respectively. The latent heat of fusion of pure nickel, 297.6 J/g (Ref. 19), was used.

The last term in Equation 3, q_i, was used to include the effect of latent heat of fusion that is absorbed and released during the melting and freezing of weld metal. In general, the latent heat release rate during weld solidification is not a constant and can be related to the compositions and cooling rate by consideration of the solidification kinetics of welding processes (Ref. 20). However, for the experimental alloy used in this study, some necessary thermophysical data were not available to allow such a treatment. The following simplified approach was used instead in the heat transfer analysis.

The solidification temperature range (1601 to 1404 K) of the alloy was evenly divided into three intervals. The latent heat was assumed to be released in these three intervals by a ratio of 7:2:1, with a major portion of the latent heat being released in the first interval:

$$q_l = \begin{cases} 0.7\dfrac{3L}{T_l - T_s}\dfrac{dT}{dt} \text{ for } T \in (1535, 1601K) \\ 0.2\dfrac{3L}{T_l - T_s}\dfrac{dT}{dt} \text{ for } T \in (1470, 1535K) \\ 0.1\dfrac{3L}{T_l - T_s}\dfrac{dT}{dt} \text{ for } T \in (1404, 1470K) \end{cases} \quad (4)$$

where L is the volumetric latent heat, and T_l and T_s are the liquidus and solidus of the alloy, respectively. This treatment was consistent with experimental observations (Ref. 21) and DTA measurement (Ref. 22) in which the solidification rate is highest in the early stages.

Mechanical Model

The mechanical responses of the superalloy specimen during the Sigmajig test were essentially treated within the confines of continuum mechanics of solids. In light of the thickness of the specimen, the problem was considered as a geometrically nonlinear plane stress problem. Nonzero stress components only exist in the plane of the specimen. In those cases where prestress was applied, the steel grips of the Sigmajig fixture were also included in the model, with the same plane stress assumption but a different thickness (38 mm). It was assumed that there was no relative displacement between the steel grips and the testing plate. This condition was enforced in the model by equating the nodal displacements of the steel grips to the corresponding ones of the specimen.

Similar to the heat transfer analysis, only half of the specimens needed to be modeled due to the symmetry with respect to the weld centerline—Fig. 2. The specimen and the steel grips were discretized with eight-node second order isoparametric quadrilateral elements with a reduced integration scheme.

As discussed earlier, the loading train of the Sigmajig test can be effectively modeled as a pair of "push" springs. Since the rigidity of the other part of the loading train (the loading bolts, for example) is much greater than that of the Bellville washers, the relative displacement of the push spring during preloading and the subsequent welding is controlled by the compliance of the washers. After some simple manipulation, the following equation was derived to describe the load and displacement relation of a push spring during welding:

$$F = 1621.4u - 19.69\sigma_o \quad (5)$$

where F (N) is the force in the spring, and u (mm) is the displacement of the spring, relative to its position after preloading. It also represents the displacement of the nodal point of the specimen that is connected with the spring; σ_o (MPa) is the prescribed stress level for a given test. In the mechanical model, it was assumed that the springs could only move along the y-direction, *i.e.*, normal to the weld centerline—Fig. 2.

For a complete anisotropic body, 21 elastic constants are required to describe the elastic stress/strain relationship. Because of the face-centered cubic structure of the single crystal superalloy, the alloy exhibits a cubic symmetry with respect to its <100> crystallographic directions. Thus, the required elastic constants reduce to three: c_{11}, c_{12}, and c_{44}. For the plane stress condition, the stress and elastic strain relation can be written as:

$$\begin{bmatrix} \sigma_{xx} \\ \sigma_{yy} \\ \sigma_{zz} \\ \sigma_{xy} \end{bmatrix} = \begin{bmatrix} c_{11} & c_{12} & c_{12} & 0 \\ c_{12} & c_{11} & c_{12} & 0 \\ c_{12} & c_{12} & c_{11} & 0 \\ 0 & 0 & 0 & c_{44} \end{bmatrix} \begin{bmatrix} \varepsilon_{xx}^{el} \\ \varepsilon_{yy}^{el} \\ \varepsilon_{zz}^{el} \\ \gamma_{xy}^{el} \end{bmatrix} \quad (6)$$

with the constraint of $\sigma_{zz} = 0$.

According to the data for several nickel-based superalloys (Refs. 19, 23, 24), the elastic constants are not strong functions of composition. Thus, the single crystal elastic constants used in this study were based on pure nickel (Ref. 25) and extrapolated for temperatures above 900 K:

$$\begin{aligned} c_{11} &= 269.9 - 0.0595T - 4\times10^{-4}T^2 \\ c_{12} &= 149.9 - 0.0024T - 9\times10^{-6}T^2 \\ c_{44} &= 135.3 - 0.038T - 1\times10^{-6}T^2 \end{aligned} \quad (7)$$

where the elastic constants are in GPa, and the temperature, T, is in Kelvin.

However, the plastic constitutive relation for the experimental single crystal alloy was not available. This study used a rather simplified temperature dependent isotropic linear work-hardening constitutive relation with a plastic modulus of $2\sigma_{ys}$. σ_{ys} is the initial yield strength of the alloy (Fig. 4), similar to those of IN-738.

The thermal expansion, $\Delta l/l$, is also shown in Fig. 4. The rapid change in thermal expansion in the solidification temperature range is related to the 5% volumetric solidification shrinkage of the alloy (Ref. 16).

As discussed in Ref. 20, the effects of solidification in the GTAW weld pool need special consideration when the mechanical responses of a welded structure are formulated on the basis of continuum

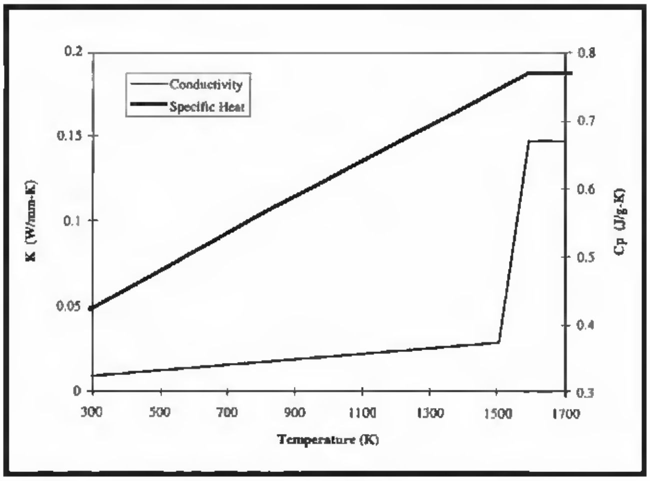

Fig. 3 — Thermophysical properties used in analysis.

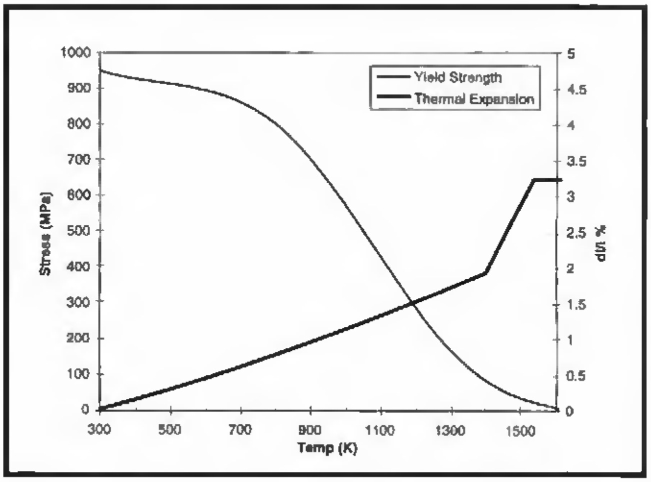

Fig. 4 — Initial yield strength and thermal expansion used for the mechanical models.

proach of Ref. 20, the effect of solidification shrinkage was treated by using the "effective" thermal expansion coefficient in the solidification temperature range. The shrinkage was assumed to be linearly distributed in the solidification temperature range and effectively treated as an additional thermal expansion/contraction term caused by temperature change. In addition, the shrinkage in the upper one-third ΔT, where ΔT is the solidification temperature range, was assumed to cause deformation in the liquid metal only, so that it was neglected in the effective thermal expansion coefficient. Similarly, the "normal" thermal expansion due to temperature change was also neglected for temperatures above 1535 K.

In place of the tedious dynamic element rebirth scheme used in Ref. 20, the other solidification effects, *i.e.*, the annihilation of plastic strain upon solidification and the change of initial temperature in thermal strain calculation, were treated by modifying the material constitutive relation in the solidification temperature range in this study. Special attention was paid to avoid the possible numerical convergence difficulties that could arise due to the drastic changes of plastic and thermal strains upon solidification. The algorithm was robust. The computational time was essentially the same as in the case in which the solidification effects were not included.

Results

Sigmajig Test

Both centerline (longitudinal) and transverse cracks were observed in this study. Figure 5 shows the welds with cracks in some selected specimens. Table 1 summarizes the occurrence of the centerline cracking under the conditions investigated. The severity of the centerline cracking is represented by the percent cracking, defined as the fraction of the specimen length cracked. As indicated in the table, the crack length and initiation point for centerline cracking depend on both the arc welding speed and the prestress level. Cracks were observed in three cases: 1) low welding speed and high prestress (4.23 mm/s, 172 MPa); 2) high welding speed and high prestress (14.8 mm/s, 172 MPa); and 3) high welding speed and zero prestress (14.8 mm/s, stress free). Cracks initiated at the weld start when the welding speed was high. On the other hand, centerline cracking did not initiate until the solidification front passed the middle point of the plate in the low welding speed tests.

The observed transverse cracks were quite unusual, since the Sigmajig test was designed for testing the susceptibility of centerline cracking. Using the stroboscopic vision system, it was observed that the initiation site for the transverse cracks was not located on the centerline of the weld. The cracks started from a location in the fusion zone close to the weld interface, as shown in Fig. 6.

The tendency for the transverse cracking seems dependent upon the welding speed only. Severe transverse cracking occurred in the high-speed welding

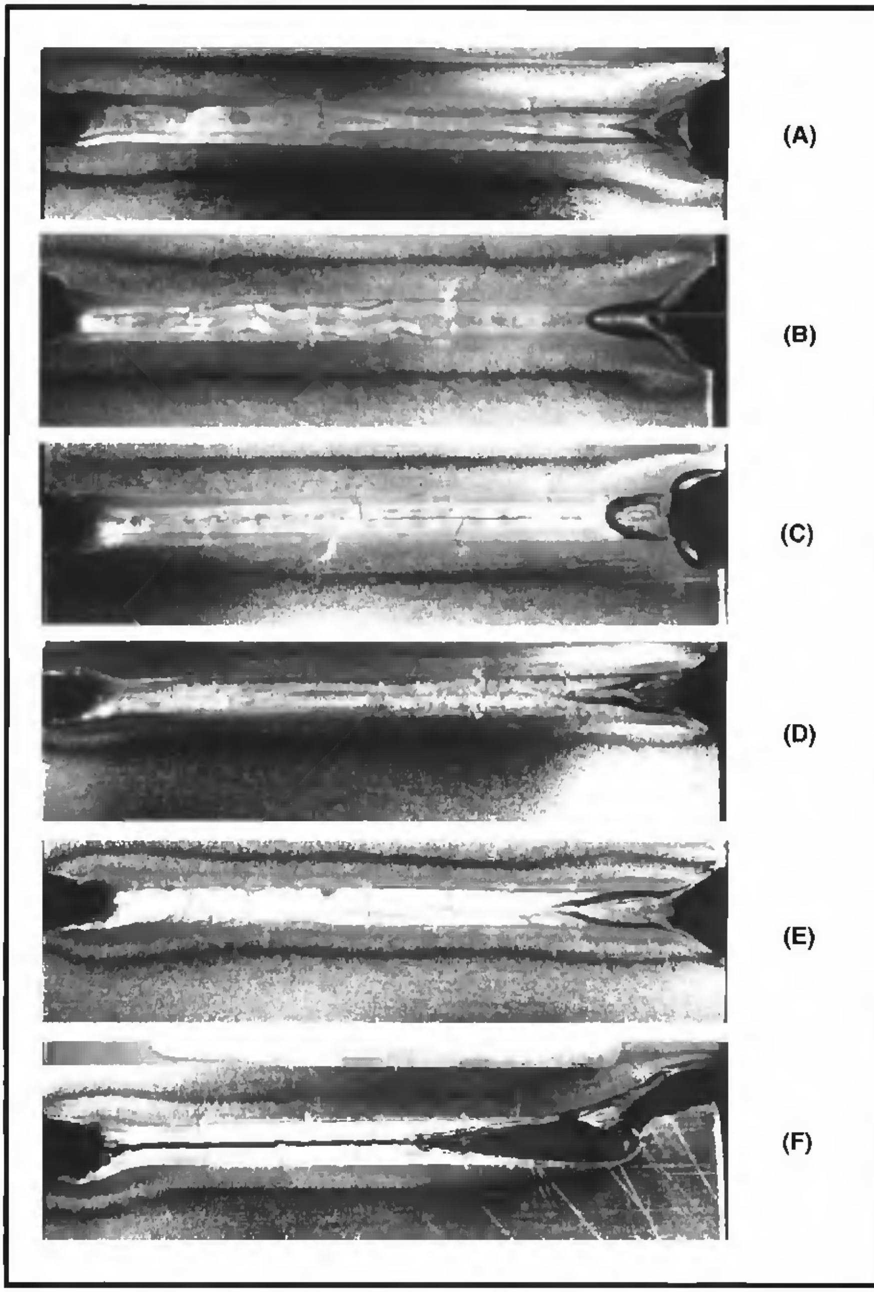

Fig. 5 — Appearance of welds and solidification cracks. Magnification: 2x. Welding direction is from left to right. A — 4.23 mm/s, free specimen; B — 4.23 mm/s, 68.9 MPa; C — 4.23 mm/s 172 MPa; D — 14.8 mm/s, free specimen; E — 14.8 mm/s, 68.9 MPa; F — 14.8 mm/s 172 MPa.

Table 1—Percent Cracking of Centerline Solidification Cracks

Prestress Level (MPa)	Welding Speed 4.23 mm/s	14.8 mm/s
Stress free	0%	15%**
68.9	0%	0%
172	50%*	100%

*Crack initiated approximately at the middle point of the weld.
**Crack initiated at the start of the weld.

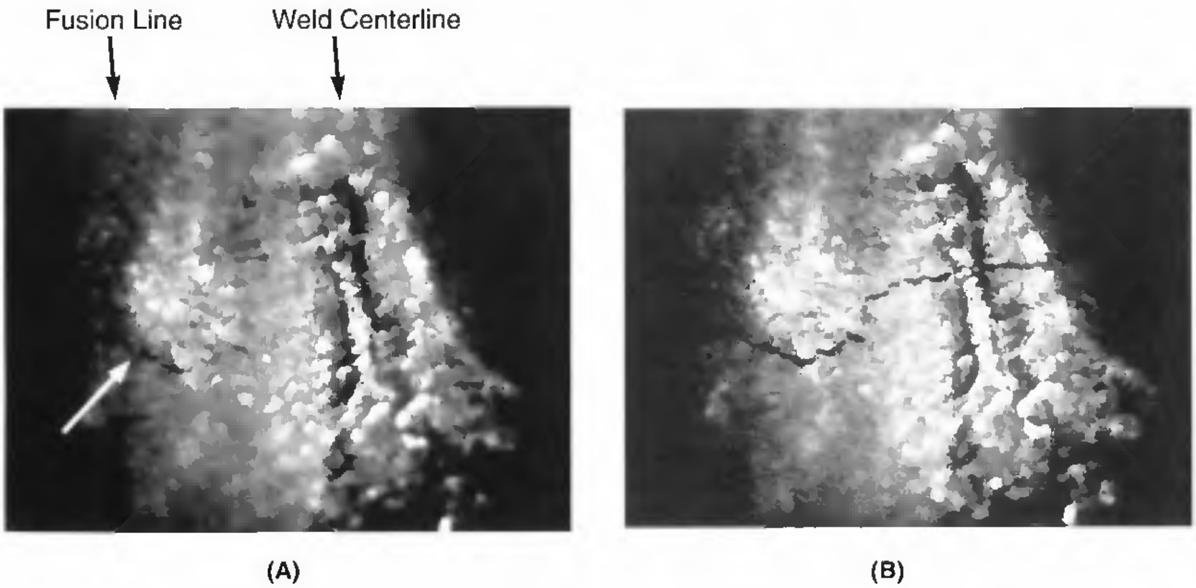

Fig. 6 — Transverse crack initiation site. A — arrow points to the crack initiation location; B — shows the same view after the crack was fully developed across the fusion zone.

(14.8 mm/s) tests with an average of seven cracks per specimen, whereas only three or less cracks were observed in each low welding speed specimen, regardless of the loading condition—Fig. 5. Note also in Fig. 5 that the transverse solidification cracks did not cross the centerline cracks, indicating that the transverse solidification cracks might initiate at a lower temperature than that of the centerline solidification cracks. In fact, it was observed that, especially in the low-speed welding tests, some transverse cracks continued to propagate in the heat-affected zone (HAZ) well after the welding was completed. Nevertheless, SEM examination revealed that the fracture surface of the transverse cracks indeed exhibited the characteristics typical of solidification cracking—Fig. 7.

Numerical Analysis

As noted earlier, the bulk liquidus and solidus temperatures measured from DTA for the alloy investigated are 1601 and 1404 K, respectively. It is expected that the actual solidus during weld metal solidification would be lower than 1404 K due to the nonequilibrium solidification process involved. Direct observation (Ref. 3) on the solidification cracking of Type 316 stainless steel has revealed that the weld centerline cracking often initiated at a location some distance behind the apparent trailing edge of the weld pool, *i.e.*, at a temperature below the bulk solidus of 316 steel (1645 K, according to Ref. 26). Solidification cracking could also initiate at a higher temperature (even reach the bulk solidus temperature when the external loading rate is high) as noted by Matsuda, *et al.* (Ref. 21). Although it is possible in principle to roughly estimate the crack initiation temperature based on the fracture surface morphology (Ref. 27), the present study did not determine the crack initiation temperature experimentally,

Fig. 7 — Typical fracture surface of transverse cracks shows characteristics of solidification cracking.

primarily because it may vary from specimen to specimen as the welding and loading conditions change. Instead, this study assumes that, depending upon the testing conditions, cracking would initiate anywhere between 1600 and 1300 K as long as the stress/strain condition and the microstructure at that particular temperature favor such an event. Therefore, this study focused on the local stress evolution over the entire temperature range between 1600 and 1300 K.

In previous studies (Refs. 20, 28), it was found that, using the modeling approach outlined earlier, the prediction of the temperature field around the weld pool is quite accurate. Therefore, experimental temperature measurement was not conducted in this study for model validation. However, the calculated weld pool size (width and length) for both welding speeds was compared with that of the actual ones. The agreement was very good as shown in Table 2.

Before discussing the local stress field around the weld pool under various testing conditions, it is worth examining first the predicted dynamic reaction of the loading springs during the test. Figures 8 and 9 show the reaction forces in the load springs as a function of time for a prestress level of 68.9 MPa. The reaction force, F, is normalized with respect to the preapplied load, F_o, in the figures. Figure 8 presents the results for the low welding speed (4.23 mm/s) and Fig. 9 for the high welding speed (14.8 mm/s). It is clear that

Table 2—Comparison of Predicted and Measured Apparent Weld Pool Size

Welding Speed, mm/s	Width, mm Measurement*	Width, mm FEM**	Length, mm Measurement***	Length, mm FEM**
4.23	4.0	4.1	n/a	9.11
14.8	3.2	3.2	18.6	18.2

*Measured under a 10X microscope.
**Used the bulk solidus temperature (1404K) as determined in the DTA.
***Based on the apparent weld pool shape of a completely separated specimen (Fig. 5F).

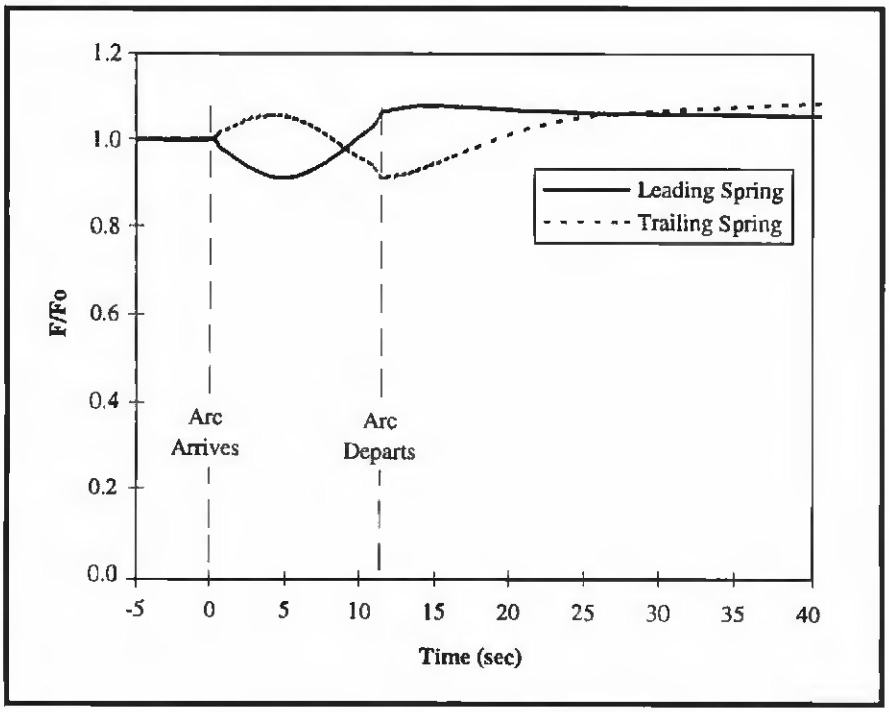

Fig. 8 — Predicted spring force vs time; 68.9 MPa and 4.23 mm/s.

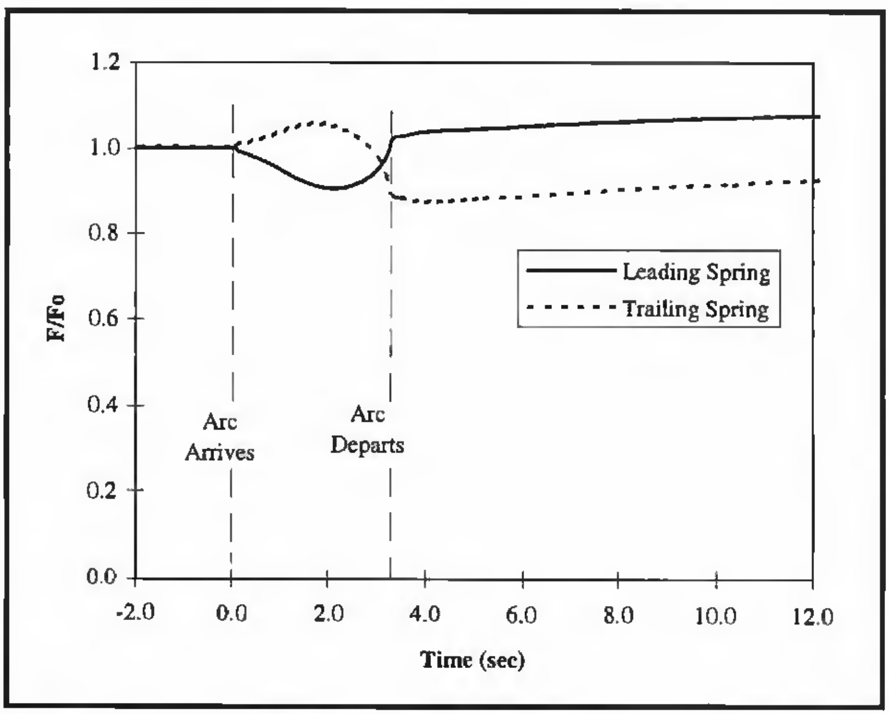

Fig. 9 — Predicted spring force vs time; 68.9 MPa and 14.8 mm/s.

the response of the loading springs depends upon the welding speed. Furthermore, they both resemble the general characteristics of the loading train's response as experimentally monitored by Goodwin (Ref. 10) for the case of low stress and no crack. The force in the spring at the starting end of the specimen (leading spring) is represented by the solid curve in the figures. It decreases first when the arc enters the specimen, reaches a minimum when the arc is approximately at the middle point of the plate, and then essentially recovers to the preloading level prior to welding as the specimen cools. The loading spring at the finishing end of the specimen (trailing spring) responds later than the first, reaches a minimum when the welding arc is about to leave the specimen, and then recovers similarly. In fact, the calculated final loads in the loading springs were compared favorably with the measured values in the loading train. For example, the calculated final loads for the low welding speed case (4.23 mm/s and 68.9 MPa) were 1370 and 1478 N for the leading and the trailing springs, respectively, whereas the corresponding measured values were 1450 and 1536 N. Thus, the reactions of the loading train in the Sigmajig test were appropriately simulated in the present analysis.

Figures 10 and 11 show the temperature and thermal stress distributions at 6.3 and 11.4 s, for the case of 4.23 mm/s and 172 MPa. The upper half of the figures shows the stress distributions, and the lower half shows the corresponding temperature distributions. Both the transverse and longitudinal stresses are shown. The scale was chosen such that the stresses in the temperature range of interest could be clearly presented. Part of the steel grips are also shown in the figures. The stress patterns in the specimen are very complex. Most importantly, a comparison of the local stress fields between the two time intervals demonstrates that the local stress distributions in the vicinity of a weld pool — particularly around the trailing edge of the weld pool — are greatly influenced by the location of the weld pool in the specimen, even for a given testing condition. When the weld pool is at the middle of the specimen (Fig. 10A), the entire solidification region (1600 to 1300 K) is immersed in a compressive transverse stress field. The maximum compressive stress zone (–60 MPa and less) covers the temperature range between 1500 and 1300 K where cracking is most likely to occur. The compressive transverse stress zone around the weld pool reduces both its extent and magnitude when the weld pool moves to the finishing end of the specimen (Fig.

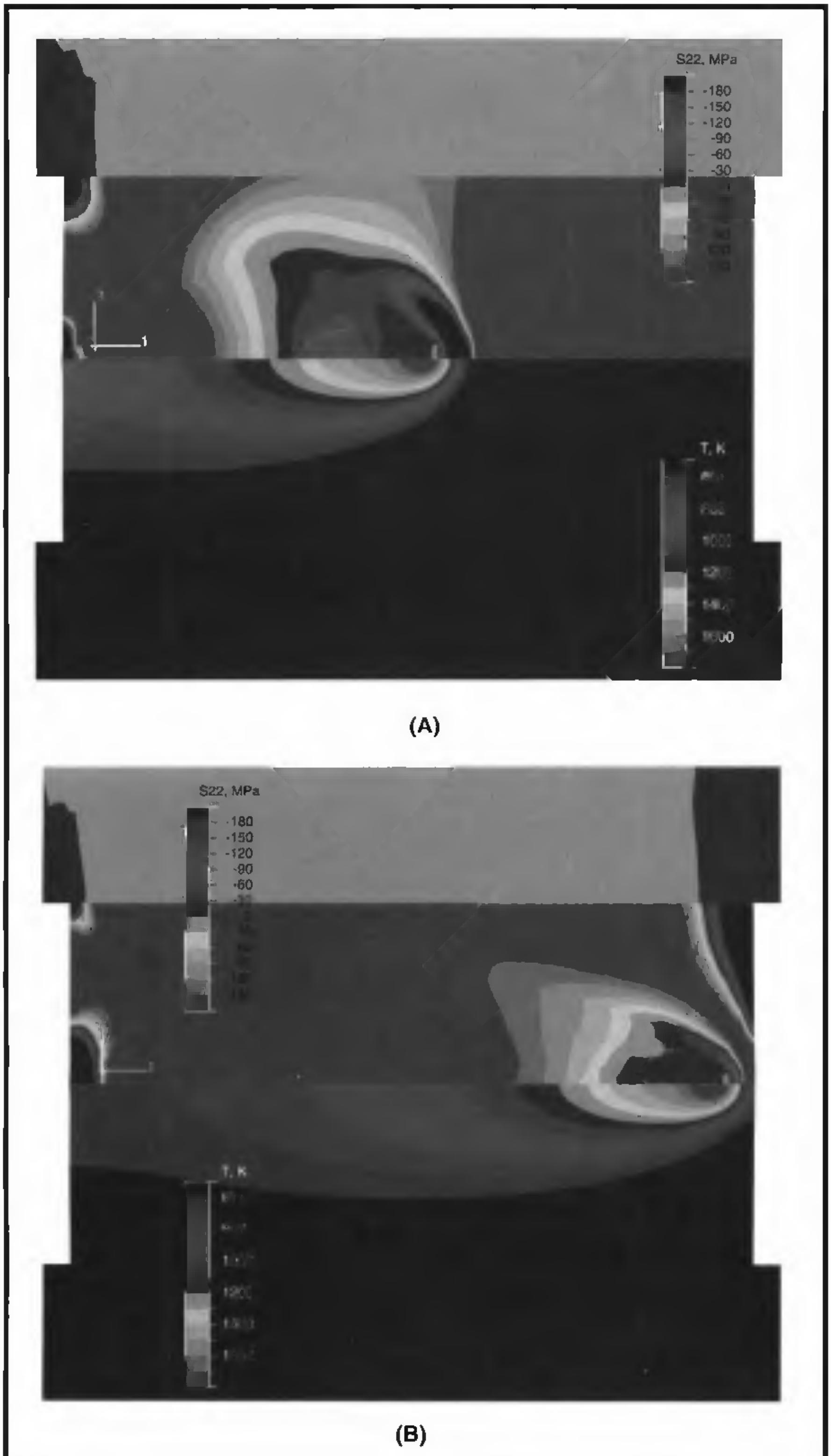

Fig. 10 — Transverse thermal stress contours and corresponding temperatures for the case of 4.23 mm/s, 172 MPa: A — at 6.3 s; B — at 11.4 s.

10B). In fact, the lower portion of the solidification temperature range (1400 to 1300 K) experiences tensile transverse stress, although the higher portion still sees a moderate compressive transverse stress (no less than –30 MPa).

Note that this type of strong spatial dependency of local stresses was exhibited in all the cases analyzed in the present study. Clearly, it forms the basis for explaining the variations in crack initiation under different testing conditions.

Discussions

As noted earlier, solidification cracking results from the competition between the material resistance to cracking and the mechanical driving force for cracking. When the mechanical driving force exceeds the material resistance, cracking occurs. In general, the material resistance to cracking depends upon the intrinsic cracking process, which is governed by variables such as the interfacial tension that determines the energy needed to separate the interdendritic bonding, the fluidity of the molten metal that determines how fast the liquid metal can fill the interdendritic region, and the dendrite morphology that determines the solid bridging of the dendrites. Any other factors that can influence these intrinsic variables will also influence the material resistance to cracking. Among the factors that strongly affect the intrinsic variables are alloy composition, solidification kinetics, cooling rate, welding parameters (heat input, welding speed), and welding process and procedure. In general, the material resistance varies from location to location, and it evolves as the solidification process goes on at a given location.

Because of the nature of weld microstructure, it is expected that the evolution of the material resistance to centerline cracking will be different from that of transverse cracking. Furthermore, the evolution of material resistance for a given cracking mode is expected to be different for different welding speeds. It is thus important to recognize that, because cracking is controlled by both mechanical driving force and material resistance, it is meaningless to use *only* the differences in mechanical driving force to assess the occurrence of cracking under different welding speeds. Likewise, the mechanical driving forces should not be directly compared between a centerline crack and a transverse crack.

On the other hand, it is reasonable to assume that the evolution of material resistance at a given location does not change for different prestress conditions. It is also reasonable to assume that the evolution of material resistance does not change once a steady weld pool is established for a given welding condition. This means that the evolution of material resistance for a given welding speed is similar along the weld centerline, except in the starting and finishing parts of the weld. Thus, if the computational model reflects the thermomechanical condi-

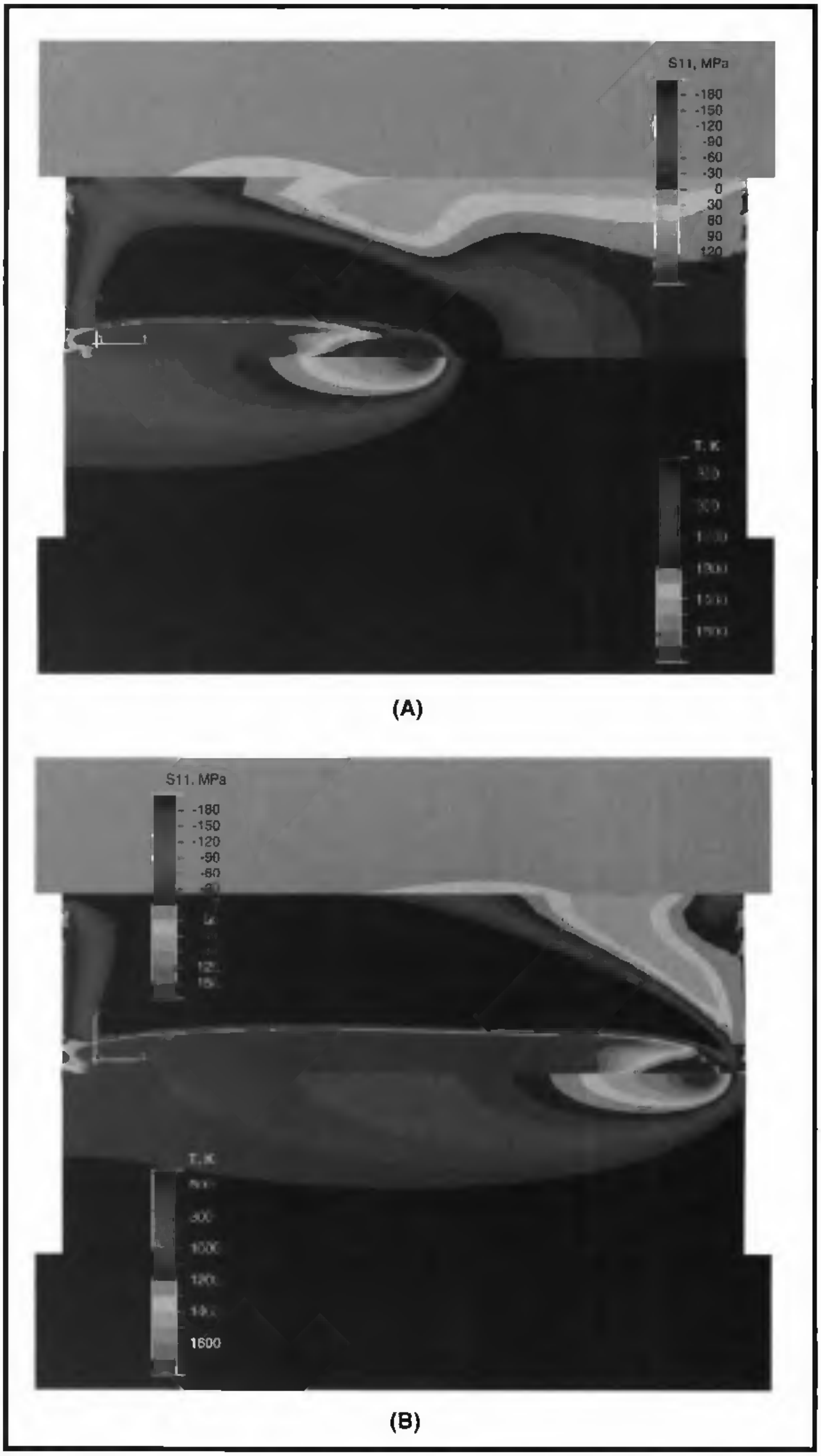

Fig. 11 — Longitudinal thermal stress contours and corresponding temperatures for the case of 4.23 mm/s, 172 MPa: A — at 6.3 s; B — at 11.4 s.

weld. Thus, if the computational model reflects the thermomechanical conditions experienced in the vicinity of the weld pool, the mechanical driving forces obtained from the analysis should be able to explain the different solidification cracking behaviors under these "comparable" material resistance conditions.

The parameters representing the mechanical driving force for solidification cracking may be a complex function of the stresses and strains in the solidification temperature range. As a first approximation, this study assumes that the stress transverse to the weld centerline is responsible for the occurrence of centerline cracking, and the longitudinal stress for transverse cracking. In addition, other parameters can also play an important role, for example, the mechanical strains accumulated in the solidification temperature range (Ref. 20).

Direct observations during the test revealed that the centerline solidification cracks appeared to initiate on the centerline of the weld. Since the evolution of transverse stresses varies from point to point along the weld centerline, it is important to examine the stress evolution for all positions along the centerline in the crack initiation temperature range. To this end, transverse stress/location/temperature diagrams were generated from the computational analysis for each of the six testing conditions—Fig. 12. The diagrams were constructed by tracing the transverse stress evolution of each nodal point on the centerline as the temperature decreases from 1600 to 1300 K. By the same procedure, the diagrams for the longitudinal stresses were constructed using a set of nodal points close to the weld interface where transverse cracks were observed to initiate. They are shown in Fig. 13. These diagrams give an overview of the variations in mechanical driving force in the solidification temperature range for the alloy studied. The effects of position, welding, and loading conditions on the mechanical driving force are clearly presented.

In general, the evolution of the transverse stress at a point on the weld centerline is such that a compressive stress is first developed upon cooling from the liquidus temperature of the alloy. In the region around the weld start, this compressive stress normally changes to a tensile stress before the completion of solidification. As the weld pool enters the middle portion of the specimen, transition to tensile stress gradually shifts down to lower temperatures. In certain loading and welding conditions, the compressive stress dominates the entire crack initiation temperature range (1600 to 1300 K). It should be noted that this general trend is consistent with other recent computational studies on the local stress distributions around a traveling weld pool (Refs. 3, 4, 20). However, the development of a second tensile stress hump after the solidification front passes the middle point of the specimen, as shown in Fig. 12, has not been reported in the past. The existence of this second tensile stress region plays an important role in explaining a fundamental cracking phenomenon ob-

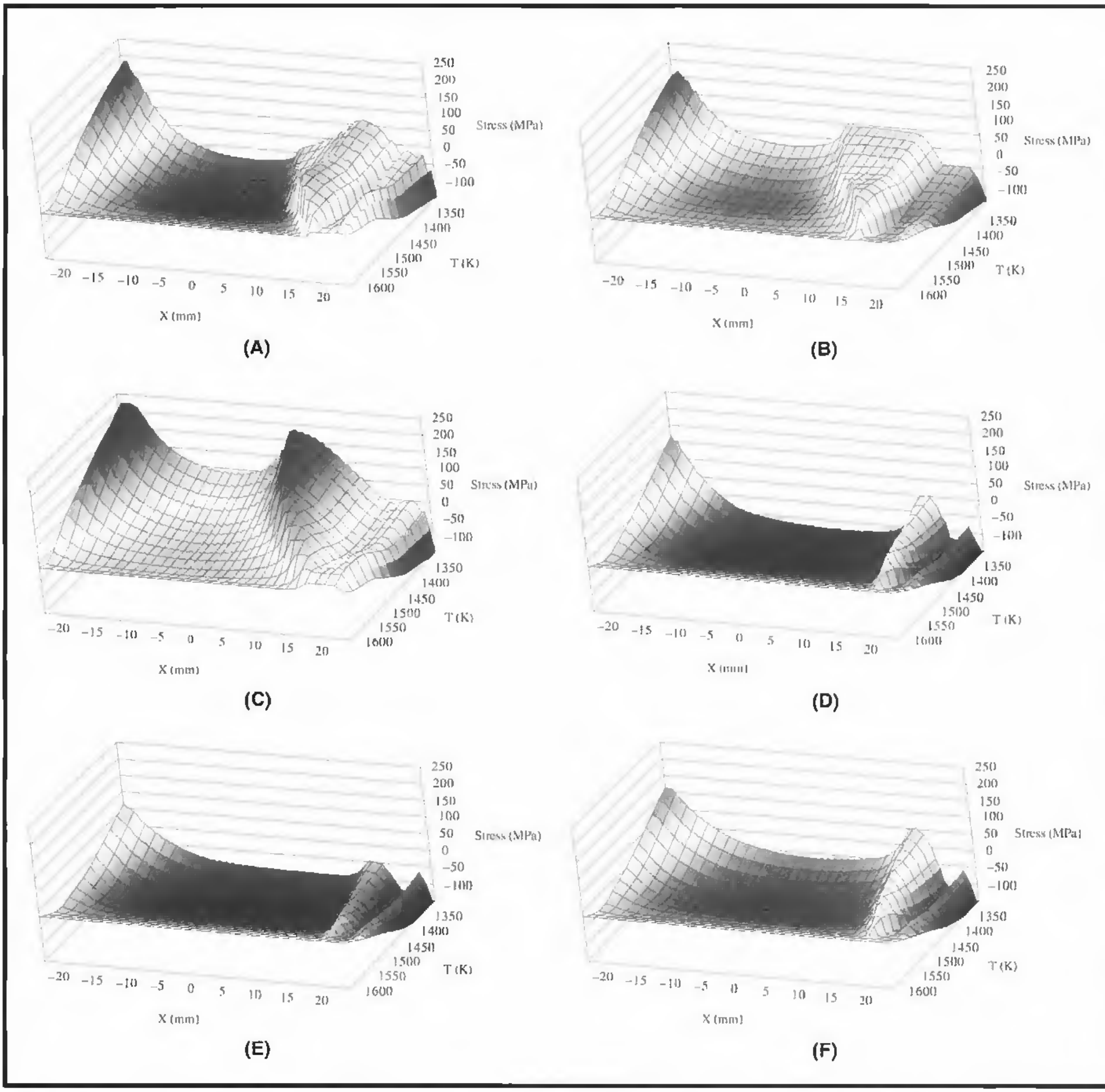

Fig. 12 — Transverse stress, location and temperature diagrams for y = 0 (weld centerline). A — 14.8 mm/s, free specimen; B — 14.8 mm/s, 68.9 MPa; C — 14.8 mm/s, 172 MPa; D — 4.23 mm/s, free specimen; E — 4.23 mm/s, 68.9 MPa; and F — 4.23 mm/s, 172 MPa.

served in the Sigmajig test, which will be discussed later.

The longitudinal stress is compressive near the liquidus temperature—Fig. 13. However, it always changes to a tensile stress before cooling down to 1300 K, regardless of the prestress levels and the welding conditions.

Stresses at the Centerline Crack Initiation Sites

In the high welding speed tests, the experiment has revealed that a centerline solidification crack, if it occurs, would initiate at the starting edge of the specimen—Fig. 5. Centerline cracks were observed in the high and low loading conditions (172 MPa and stress free specimens), while the medium loading condition (68.9 MPa) did not cause any centerline crack. Intuitively, it is difficult to comprehend why centerline cracking occurs in the stress-free specimen but not in a moderately prestressed specimen based on the threshold prestress concept. However, this phenomenon can be readily interpreted in terms of the local stress evolution at the starting edge of the specimen where the centerline crack initiates. According to the diagrams of Fig. 12A–C, a tensile transverse stress field develops at the weld start for all three loading conditions used in the high welding speed tests. The maximum tensile stress is located at about 2.5 mm from the edge of the specimen. For a better comparison, Fig. 14 plots the transverse stress evolution at that location only. Compressive

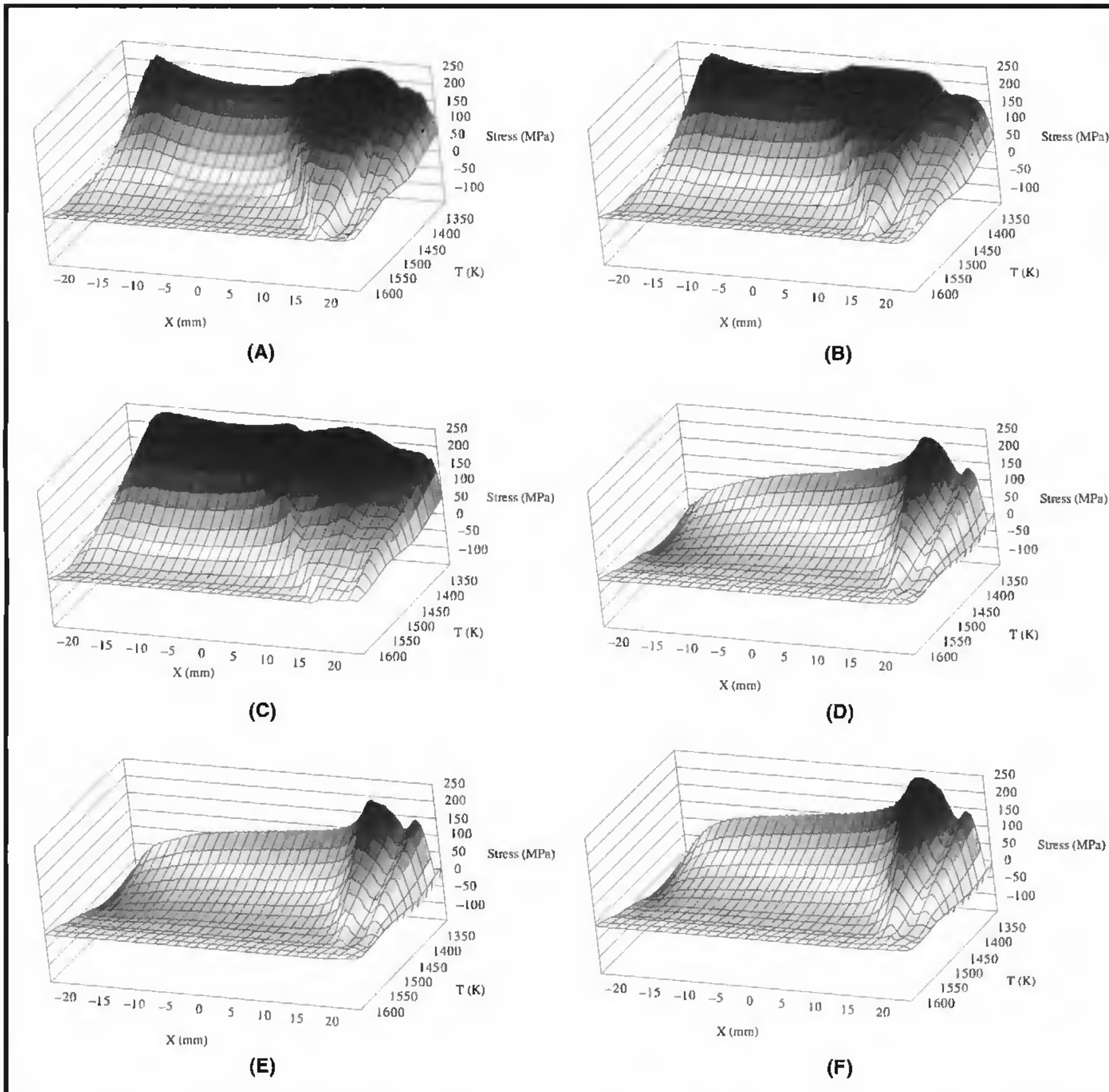

Fig. 13 — Longitudinal stress, location and temperature diagrams. A — 14.8 mm/s, free specimen; B — 14.8 mm/s, 68.9 MPa; C — 14.8 mm/s, 172 MPa; D — 4.23 mm/s, free specimen; E — 4.23 mm/s, 68.9 MPa; and F — 4.23 mm/s, 172 MPa.

transverse stresses were initially developed there upon solidification from 1600 K, then changing to tension before temperature drops to 1500 K for all three prestress conditions. However, the tensile stress in the 68.9 MPa case is always lower than the other two cases over the entire crack initiation temperature range. Therefore, the initiation behaviors of the centerline cracking during the high welding speed tests are well explained in terms of the transverse stress evolution at the crack initiation site.

The tendency for centerline cracking under the low welding speed was found to be different. Centerline solidification cracking was observed only in the 172 MPa case. During welding, the centerline cracking was initiated somewhere between 25 to 30 mm from the starting edge of the weld. According to the computational results (Fig. 12D–F), except in the weld start region, the first half of the weld centerline is subjected to a very strong compressive stress field in the entire crack initiation temperature range. Transition toward a tensile stress field begins only after the solidification front passes approximately the middle point of the specimen, as indicated by the humps in the stress/temperature/location diagrams. However, only in the 172 MPa case does the tensile transverse stress field fully develop. For the stress free specimens, the transverse stress becomes tensile only at one nodal point (x = 15 mm) over the entire weld centerline, and not at all in the 68.9 MPa specimens—Fig. 15.

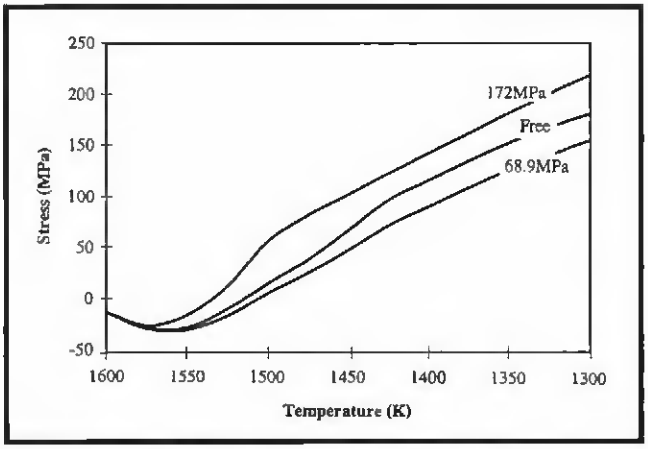

Fig. 14 — Transverse stress evolution responsible for centerline cracking initiation at the starting edge of the specimen; x = –22.5 mm, 14.8 mm/s.

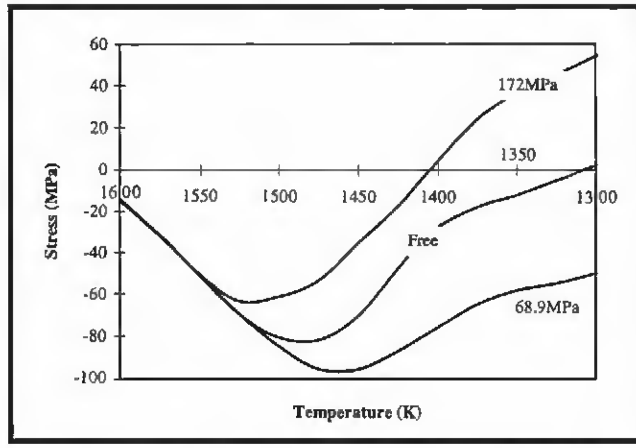

Fig. 15 — Transverse stress evolution at x = 15 mm, 14.8 mm/s.

According to Fig. 12, a tensile stress region begins to develop at a location about 37.5 mm from the weld starting edge (x = 12.5 mm) when the temperature approaches 1300 K for the 172 MPa case. Compared with experimental observation, the predicted cracking initiation site is about 5 mm further away from the weld starting edge.

As mentioned earlier, a fundamental characteristic of centerline solidification cracking in the Sigmajig test is that it is very rare to have a crack length between 60 to 100% (Ref. 10). This means that a centerline crack normally does not initiate until the solidification front passes the middle point of the specimen. If the prestress is sufficiently high, the crack initiates at the start of the weld, followed by a complete specimen separation (100% cracking). This phenomenon has been attributed to the variations in the reaction force in the loading train, as monitored with a strip-chart recorder during the test (Ref. 10). However, based on the results of the present work, a new explanation is proposed. The initiation of a centerline crack is directly related to the second transverse stress hump located after the middle point in the specimen in the stress/location/temperature diagrams. According to Fig. 12, the site where the hump first breaks into tension would be located between x = 15 mm and x = 20 mm (about 40 to 45 mm from the starting edge of the specimen) in the low welding speed cases. The transition to tension is closer to the middle point of the specimen in the high welding speed cases. Obviously, if a centerline crack does not initiate at the start of the weld, then it will not initiate until a tensile transverse stress appears again in the hump. As the prestress further increases, the transition position in the hump shifts toward the middle point of the specimen, creating a longer centerline crack.

Note that the humps not only appear when a prestress is applied, but also in the stress free specimens. Therefore, it can be argued that the variations of the reaction force in the loading train are not the dominant factor to cause the existence of the hump and thus the absence of a 60 to 100% longitudinal centerline crack. Careful examination of the calculated temperature field indicates that the front of the weld pool is very close to the end of the specimen when a hump begins to develop—Fig. 10B. A more reasonable explanation is thus related to the interaction between the weld pool and the free edge of the specimen. When the weld pool is in the middle of the specimen (Fig. 10A), there is a sufficient ligament of material between the front of weld pool and the finishing edge of the specimen. This ligament is not yet exposed to elevated temperatures and thus is high in strength and rigidity. This rigid ligament prohibits the free outward expansion of the weld pool and favors the development of compressive stresses in the vicinity of the weld pool. As the front of the weld pool approaches the finishing edge of the specimen, the material in front of the weld pool becomes very hot and soft and cannot prevent the free expansion of the weld pool and the adjacent areas. Therefore, the weld pool effectively opens up and promotes the chance for its trailing edge to experience a tensile stress field.

Transverse Cracking

Figure 11 reveals that the front side of the weld pool is immersed in a compressive longitudinal stress field. For the locations of the same distance from the weld starting edge, tensile stress begins to develop first at a location close to the weld interface. This type of stress distribution favors the initiation of transverse cracks at a location close to the interface, which is consistent with the experimental observations as mentioned earlier.

The longitudinal stress evolution is shown in Fig. 13. The first striking feature is that, unlike the transverse stress, the longitudinal stress evolution is essentially independent of the prestress (the mechanical restraint conditions) for the two welding speeds used in this study. This is reflected in the weldability test by the fact that the severity of transverse cracking was not influenced by the magnitude of the prestress—Fig. 5.

The second feature observed in Fig. 13 is that there are subtle differences in both the magnitude and the distribution of the longitudinal stress for the two welding speeds. In the case of high speed welds, as shown in Fig. 13A–C, the buildup of the longitudinal stress quickly reaches the maximum level, and this maximum stress is maintained through the length of the weld, except in the regions representing the starting and terminating craters. As noted earlier, the material resistance in the locations covered by this maximum stress plateau would not vary. Therefore, it is expected that the transverse cracks, if formed, would be located either prior to or as soon as the plateau is reached. As shown in Fig. 13, the longitudinal stress evolution reaches the plateau at a location about 7.5 mm from the weld starting edge of the specimen which is comparable to the location where the first transverse crack was observed—Fig. 5.

In the case of low welding speed tests (Fig. 13D–F), the buildup of the maximum longitudinal stress occurs well into the length of the weld and close to the finishing end of the weld. Also, the maximum stress attained in the low-speed welds is much lower than the high-speed welds. The gradual buildup of the longitudinal stress evolution from the starting end to the finishing end of the weld made it possible for the transverse solidification cracking to initiate at locations away from the weld starting edge of the specimen, as observed in the tests.

Effect of Restraint in Sigmajig Test

As already mentioned, centerline cracking in the stress free specimen was not expected since the measured threshold stress for cracking was in excess of 68.9 MPa. This can be attributed to the restraining effect of the steel grips in the Sigmajig test, as explained below.

According to the principle of heat conduction, the welding heat input from the arc needs time to diffuse from the weld pool into the adjacent HAZ and base metal. As shown in Fig. 10, while the temperature at the trailing edge of the weld pool begins to decrease (on cooling), the temperature in the surrounding base metal and HAZ is still rising (on heating). Thus, the base metal and the HAZ are still in the expansion stage. The thermal expansion of the base metal and HAZ can be partially relieved in the weld pool, since the weld pool is the most deformable region in the specimen due to the low stiffness of material at elevated temperatures. For a freestanding specimen without any restraint, the thermal expansion can also be relaxed by the movement toward the free edges of the specimen. For the free prestress Sigmajig specimen used in this study, the upper half of Fig. 16 clearly demonstrates that the transverse movement in the region around the trailing edge of the weld pool is toward the weld centerline. This is consistent with many experimental observations of the inward transverse movement of the interface (Refs. 6, 29, 30). Also shown in the figure is the opposite movement of the upper edge of the specimen, which would be otherwise prohibited by the steel grips. Hence, it can be reasoned that the thermal expansion in the adjacent base metal and HAZ will push the weld fusion boundary inward to the centerline of the weld, and this inward movement is enhanced if the specimen is constrained by the steel grips. A related analysis (Ref. 2) also reported similar restraining effects on the fusion boundary movement. This explanation is also supported by the high-tensile transverse stress at the weld starting edge of the specimen in this study. Therefore, the steel grips used in the Sigmajig test not only serve as part of the loading train to apply the prescribed load to the specimen, but also act as a restraining fixture that prevents the free thermal expansion of the specimen during welding and retards the development of tensile transverse stresses in the solidification temperature range.

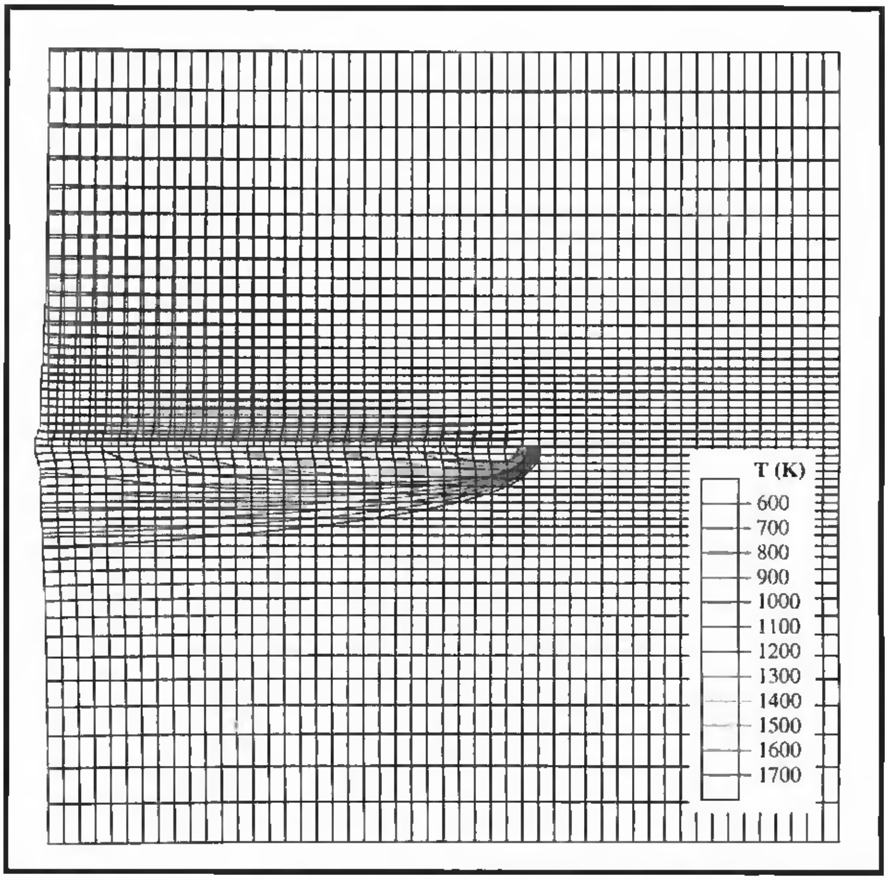

Fig. 16 — Deformation of the Sigmajig specimen at t = 2s; 14.8 mm/s, restraint free (dotted lines = undeformed mesh). The bottom half shows the temperature distribution. The region around the trailing edge of the weld pool moves toward the weld centerline, and the opposite movement in the region away from the centerline. Displacement magnification: 5x.

A common practice used in solidification cracking prevention is to minimize the restraint effects from the fixtures during welding, but the results of this study indicate that the restraining effect could be beneficial if applied correctly. Therefore, the proper placement of restraint by means of local heating and mechanical rolling needs to be further exploited.

Finally, note that the local stresses calculated in this study were based on the finite element formulation of continuum solid mechanics. In this regard, the local stresses are still the macroscopic "continuum" stresses in nature. The analysis cannot reveal the microscopic stresses that act on the dendrite bridges and cause the separation of the dendrites. However, the results of the present investigation suggest a postulate that deformations at the microscopic level are controlled, to a significant degree, by the development of the macroscopic stress/strain conditions in the vicinity of a weld pool. It is important to recognize that, under this postulate, it is possible to use computational models like the one presented in this work to systematically investigate the solidification cracking behaviors under various welding conditions. The fact that the calculated thermal stress results correlate very well with the experimental observations clearly provides strong support for such a postulate.

Conclusions

In this study, the solidification cracking behaviors of a nickel-based superalloy single crystal in the Sigmajig weldability test have been investigated. A finite element model has been developed to evaluate quantitatively the thermomechanical conditions for the weld metal solidification cracking phenomenon. Stress/temperature/location diagrams were constructed that reveal the complex local stress development at the trailing edge of the moving weld pool. Based on the concept of the material resistance to cracking vs. the mechanical driving force for cracking, the calculated local stress evolution in the solidification temperature range provided a good explanation for the experimentally observed solidification cracking initiation behaviors under different testing conditions.

1) The nickel-based superalloy single crystal shows severe solidification cracking susceptibility under the testing conditions investigated. Both centerline and transverse cracks were observed in the tests. The initiation of centerline cracks is strongly influenced by the loading condition and the welding speed, with decreased cracking tendency under lower welding speed. However, the formation of transverse cracks is primarily affected by the welding speed. High welding speed promotes transverse cracking.

2) The development of transverse stress is strongly influenced by the constraining effect of the loading fixture. When the prestress is low, this restraint effectively retards the development of tensile stress in the solidification temperature range so that the weld experiences a lower tensile stress than in the fixture-free case. This leads to the observation of centerline cracking that occurs in the fixture-free test, not in the moderately preloaded test.

3) The interaction between the front of the moving weld pool and the edge of the specimen promotes the formation of a tensile transverse stress field as the weld pool advances toward the end of the specimen.

4) The development of high-tensile longitudinal stress in the solidification temperature range provides the necessary mechanical condition for the formation of transverse cracks in the fusion zone. In agreement with the observed tendency of transverse cracking, the computational results show that the development of the longitudinal stress strongly depends upon the welding speed and is essentially independent of the preloading levels. The quick development of the maximum longitudinal stress plateau in the high-speed welding case, as opposed to the gradual buildup in the low-speed welding case, explains the difference in cracking severity at the two welding speeds.

Acknowledgments

The authors thank Dr. G. M. Goodwin for many helpful discussions related to this work and Dr. M. L. Santella for reviewing this paper. Thanks also go to D. McCoy for final manuscript preparation and K. Spence for editing. This research was supported by the Division of Materials Sciences, U.S. Department of Energy, under contract DE-AC05-84OR21400 with Lockheed Martin Energy Systems, and by an appointment to the Oak Ridge National Laboratory Postdoctoral Research Associates Program administered jointly by the Oak Ridge Institute for Science and Education and Oak Ridge National Laboratory.

References

1. Apblett, W. R. and Pellini, W. S. 1954. Factors which influence weld hot cracking. *Welding Journal* 33(2): 83-s to 90-s.

2. Feng, Z. and Tsai, C. L. 1993. Modeling of thermomechanical conditions at weld pool. *International Conference Proceedings on Modeling and Control of Joining Processes*, pp. 525–532.

3. Zacharia, T. 1994. Dynamic stresses in weld metal hot cracking. *Welding Journal* 73(7): 164-s to 172-s.

4. Brooks, J. A., Dike, J. J. and Krafcik, J. S. 1993. On modeling weld solidification cracking. *International Conference Proceedings on Modeling and Control of Joining Processes*, pp. 174–185.

5. Johnson, L. 1974. Moiré techniques for measuring strains during welding. *Exp. Mech.* (4): 145–151.

6. Chihoski, R. A. 1979. Expansion and stress around aluminum weld puddles. *Welding Journal* 58(9): pp. 263-s to 276-s.

7. Daytlov, V. I. and Sidoruk, V. S. 1966. The effect of the welding technique on the formation of longitudinal hot cracks. *Autom. Weld.* (3): 21–26.

8. Matsuda, F., Nakagawa, K., Kohmoto, H., Honda, Y., and Matsubara, Y. 1983. Quantitative evaluation of solidification brittleness of weld metal during solidification by in-situ observation and measurement (Report II) — Solidification ductility curves for steels with the MISO technique. *Trans. JWRI* 12(1): 73–80.

9. Dixon, B. 1993. Tests for weld metal solidification cracking — a review. *Aus. Welding Journal* (Summer): 16–22.

10. Goodwin, G. M. 1987. Development of a new hot-cracking test — the Sigmajig. *Welding Journal* 66(2): 33-s to 38-s.

11. Maziasz, P. J., Goodwin, G. M., Liu, C. T., and David, S. A. 1992. Effects of minor alloying elements on the welding behavior of FeAl alloys for structural and weld overlay cladding applications. *Scr. Metall.* 27(12): 1835–1840.

12. ASM International. 1990. *Metals Handbook*, 10th edition, Vol. 1, p. 982. Materials Park, Ohio.

13. Hibbitt, H. D., and Marcal, P. V. 1973. A numerical, thermomechanical model for the welding and subsequent loading of a fabricated structure. *Computers & Structures* 3: 1145–1174.

14. Feng, Z., Zhu, Y. Y., Zacharia, T., Fields, R. J. , Brand, P. C., Prask, H. J., and Blackburn, J. 1995. Modeling and validation of residual stress distribution in a HSLA-100 disk. *Proc. 4th Int. Conf. on Trends in Welding Research*, (eds., H. B. Smartt, J. A. Johnson and S. A. David), ASM International, 105–110.

15. *ABAQUS Theory Manual*, Version 5.4. 1994. Hibbitt, Karlsson & Sorensen, Inc.

16. ASM International. 1990. *Metals Handbook*, 10th edition, Vol. 1, pp. 950–1006. Materials Park, Ohio.

17. Touloukian, Y. S. 1966. *Thermophysical Properties of High Temperature Solid Materials*, Vol. 2, Part 2.

18. Touloukian, Y. S., Powell, R. W., Ho, C. Y., and Klemens, P. G. 1970. *Thermophysical Properties of Matter*, Vol. 1, IFI/Plenum, New York, N.Y.

19. Touloukian, Y. S., and Ho, C. Y. (eds.) 1981. *Properties of Selected Ferrous Alloying Elements*. McGraw-Hill, New York, N.Y.

20. Feng, Z. 1994. A computational analysis of thermal and mechanical conditions for weld metal solidification cracking. *Welding in the World*, 33(5): 340–347.

21. Matsuda, F., Nakagawa, H., and Sorada, K. 1982. Dynamic observation of solidification and solidification cracking during welding with optical microscope (1) — solidification front and behavior of cracking. *Trans. JWRI* 11(2): 67–77.

22. Feng, Z., Zacharia, T., and David, S. 1997. On the thermomechanical conditions for weld metal solidification cracking. *Mathematical Modeling of Weld Phenomena* III, (eds., H. Cerjak, H. K. D. H. Bhadeshia), The Institute of Materials, pp. 114–148, London, U.K.

23. Hellwege, K-H. (ed.) 1979. *Landolt-Böenstein New Series* Group 3, Vol. 11. Springer-Verlag, Berlin.

24. Hellwege, K-H. (ed.) 1984. *Landolt-Böenstein New Series* Group 3, Vol. 18. Springer-Verlag, Berlin.

25. Ledbetter, H. M., and Reed, R. P. 1973. Elastic properties of metals and alloys, I. Iron, nickel and iron-nickel alloys. *J. Phys. Chem. Ref. Data* 2(3): 531–617.

26. ASM International. 1990. *Metals Handbook*, 10th edition, Vol. 1, p. 871. Materials Park, Ohio.

27. Arata, Y., Matsuda, F., Katayama, S., and Ogata, S. 1977. Solidification crack susceptibility in weld metals of fully austenitic stainless steels (Report III) — Effect of strain rate on cracking threshold in weld metal during solidification. *Trans. JWRI* 6(2): 197–207.

28. Z. Feng, Internal Research Report, Edison Welding Institute, 1997.

29. Johnson, L. 1973. Formation of plastic strains during welding of aluminum alloys. *Welding Journal* (7): 298-s to 305-s.

30. Matsuda, F., Nakata, K., and Harada, S. 1980. Moving characteristics of weld edges during solidification in relation to solidification cracking in GTA weld of aluminum alloy thin sheet. *Trans. JWRI* 9(2): 225–235.